Predictive therapeutic planning for irreversible electroporation treatment of spontaneous malignant glioma

Paulo A. Garcia*,a)
School of Biomedical Engineering and Sciences, Virginia Tech – Wake Forest University, Blacksburg, VA 24061, USA
Laboratory for Energy and Microsystems Innovation, Department of Mechanical Engineering, Massachusetts Institute of Technology, Cambridge, MA 02142, USA

Bor Kos*
Faculty of Electrical Engineering, University of Ljubljana, Trzaska 25, 1000 Ljubljana, Slovenia

John H. Rossmeisl Jr.
School of Biomedical Engineering and Sciences, Virginia Tech – Wake Forest University, Blacksburg, VA 24061, USA
Department of Small Animal Clinical Sciences, Virginia-Maryland Regional College of Veterinary Medicine, Blacksburg, VA 24060, USA
Veterinary and Comparative Neuro-oncology Laboratory, Virginia-Maryland Regional College of Veterinary Medicine, Blacksburg, VA 24060, USA

Denis Pavliha and Damijan Miklavčič
Faculty of Electrical Engineering, University of Ljubljana, Trzaska 25, 1000 Ljubljana, Slovenia

Rafael V. Davalos
School of Biomedical Engineering and Sciences, Virginia Tech – Wake Forest University, Blacksburg, VA 24061, USA

(Received 16 August 2016; revised 14 April 2017; accepted for publication 7 May 2017; published 25 July 2017)

Purpose: Irreversible electroporation (IRE) has been developed as a promising minimally invasive treatment to ablate spontaneous brain tumors with pulsed electric fields in canine patients. The purpose of the study is to determine the Peleg-Fermi parameters needed to incorporate pulse number and pulse duration into the therapeutic planning of IRE.
Methods: Seven canine patients were treated with IRE for spontaneous malignant glioma with MRI-based treatment planning. The treatment planning method consists of building patient-specific finite element models and using them to compute electric fields used in the IRE treatment. We evaluate the predictive power of tumor coverage with electric field alone vs. cell kill probability using radiographically confirmed clinical outcomes.
Results: Results of post-treatment diagnostic imaging, tumor biopsies, and neurological examinations indicated successful tumor ablation without significant direct neurotoxicity in six of the seven dogs. Objective tumor responses were seen in four (80%) of five dogs with quantifiable target lesions according to RANO criteria. Two dogs experienced survivals in excess of 1 yr, including one dog that resulted in complete response to IRE treatment for 5+ years to date. Tumor fraction exposed to electric field over 600 V/cm was between 0.08 and 0.73, while tumor fraction exposed to electric field over 300 V/cm was between 0.17 and 0.95. Probability of cell kill of $\geq$ 90% was found in tumor volume fractions between 0.21 and 0.99.
Conclusions: We conclude that IRE is a safe and effective minimally invasive treatment for malignant glioma and can be predicted with the Peleg-Fermi cell kill probability function. A tumor coverage of $\geq$ 0.9 at a cell kill probability $\geq$ 90% can be used to guide IRE treatments of spontaneous malignant glioma based on the radiographically confirmed clinical outcomes achieved. © *2017 The Authors. Medical Physics published by Wiley Periodicals, Inc. on behalf of American Association of Physicists in Medicine.* [https://doi.org/10.1002/mp.12401]

Key words: brain tumor, minimally invasive, neurosurgery, pulsed electric fields, treatment planning

1. INTRODUCTION

Malignant gliomas, especially glioblastoma multiforme (GBM), are among the most aggressive human malignancies. Patients suffering from this disease have poor prognosis with a 5-yr survival rate of about 10%.[1] The median survival for patients with GBM is only 15 months even with singular or multimodal therapy consisting of surgical resection, radiation therapy, and/or chemotherapy.[1,2] Despite development of novel therapies for treatment of malignant glioma in transgenic and genetically engineered rodent glioma models, few therapeutic advances have emerged that drastically improve survival for patients with aggressive, high-grade gliomas.[3] An obstacle for the translation of therapeutic developments into humans is the inability of the animal model to reliably reproduce the phenotypically and genotypically diverse tumor

population that is observed in humans. Therefore, developing treatment technologies in a glioma model system of a meaningful size that faithfully reproduces the human disease is critical for improving the outcome of brain cancer patients.

Canine patients with spontaneous brain tumors have been recognized for their promise as a large translational glioma model for preclinical assessment and development of novel therapeutics.[4] In dogs with several types of brain tumors, statistics on median survivals of 0.2, 0.9, and 4.9 months Statistics have been reported after receiving either symptomatic therapy, cytoreductive surgery, or multimodal therapy (radiotherapy and surgery or hyperthermia) respectively.[5] These statistics demonstrate the poor long-term prognosis for dogs with brain tumors and the urgent need for the development of more effective therapies.[5] There are substantial clinical, epidemiological, cytogenetic, and pathophysiological similarities between human and canine brain tumors that have been identified.[6] The role and value of dogs with spontaneous brain tumors in the development of experimental therapeutics has been demonstrated. Seminal work in dogs with spontaneous gliomas illustrated the feasibility and importance of real-time imaging monitoring of convection-enhanced delivery (CED) for confirmation of target coverage, as well as providing an opportunity to detect and remedy any local adverse effects of CED treatment, including reflux.[7] A preclinical study investigating dendritic cell vaccination of glioma-bearing dogs with tumor cell lysates containing a toll-like receptor ligand adjuvant in combination with *in situ* adenoviral interferon-gamma gene transfer demonstrated sufficient safety and promise to result in rapid translation of this immunogenetic therapy to a human glioblastoma clinical trial,[8] and promising active immunotherapeutic approaches using dogs with intracranial meningiomas have recently been published. Canine patients with spontaneous disease are thus an attractive preclinical model since the size and heterogeneity of their gliomas closely reproduce the characteristics of brain tumors in humans.

Recently, we demonstrated the safety and feasibility of irreversible electroporation (IRE) for the treatment of spontaneous intracranial gliomas in canine patients using patient-specific therapeutic planning.[9] IRE is a new, safe, and effective minimally invasive nonthermal ablation modality with the potential to treat unresectable tumors such as many gliomas in close proximity to critical structures.[10–14] An IRE treatment involves placing minimally invasive electrodes within or around the tumor tissue and delivering a series of short high voltage electric pulses to the targeted tumor tissue.[15–17] The exposure of the tumor to pulsed electric fields destabilizes the membranes of the cancer cells, achieving death in a precise and controllable manner with cell-scale resolution.[16,18–20]

In order to guide the physicians and veterinarians performing electroporation-based therapies, anatomically accurate numerical models have been developed for maximizing tumor coverage while minimizing damage to surrounding healthy tissue during pulse delivery.[21–24] The pulse parameters employed in the clinical study were determined from patient-specific computational models of the electric field distributions due to the sensitive nature of the intracranial environment.[9,25] In these models, as in many other studies of electroporation technologies, the electric field distribution was used to determine the tumor coverage based on electric field threshold values.[21,26–30] The imaging-based treatment planning model developed for each canine patient dictated the surgical approach for intracranial electrode placement. The models also helped determine the voltages that needed to be applied assuming a lethal electric field threshold of 500 V/cm that was determined from magnetic resonance imaging (MRI) reconstructions of IRE ablation zones with ninety 50-μs pulses in normal brain.[9,28] The radiographically confirmed clinical outcomes demonstrate that we achieved two complete responses (CR), two stable diseases (SD), and one partial response (PR) after IRE therapy of the malignant gliomas in the five canine patients that were treated with curative intent.

The goal of this study is to further refine the imaging-based computational models to explicitly incorporate additional critical treatment parameters such as pulse number and pulse duration to improve the predictive power of the cell kill distribution during the therapeutic planning procedure which can serve to improve treatment planning for brain tumors in the future.[31–33] Specifically, we correlate the radiographically confirmed clinical outcomes with advanced modeling approaches to provide the clinical community with predictive planning tools for IRE treatment of intracranial glioma.

2. MATERIALS AND METHODS

2.A. Study design and canine patient population for clinical study

This was a single-center, prospective study conducted to assess the safety and feasibility of using the NanoKnife System for ablation of spontaneous canine intracranial gliomas with irreversible electroporation.[9] Canine patients were treated according to the standards in the Guide for Care and Use of Laboratory Animals, and were approved by the institutional animal care and use committee and the Virginia-Maryland College of Veterinary Medicine clinical review board. Candidates for this study consisted of client-owned dogs with suspected spontaneous telencephalic gliomas based on MRI evaluation and tumors were biopsied and histologically confirmed prior to IRE treatment (Table I). For inclusion, canine patients were required to undergo a diagnostic MRI within 2 weeks of enrollment showing a single telencephalic intra-axial mass lesion with imaging characteristics consistent with glioma,[34] have stable neurological and cardiopulmonary functions, and have no evidence of substantial hepatic or renal dysfunction or concurrent systemic malignancy. Any type of radiotherapy treatment of the brain tumor was prescribed as exclusion criteria. A passive approach was used to enroll cases following identification from the routine clinical population presented to the Veterinary Teaching Hospital or its referral partners. The recruitment of each

patient occurred after the principal investigator's clinical review of each potential candidate. Clients provided written, informed consent for their canine patients to receive irreversible electroporation treatments. The population with intent-to-treat was defined as those clinical cases in which the NanoKnife electrode (www.angiodynamics.com) probes were inserted into the brain tissue. The specific IRE treatment protocols, electrode configuration, and tumor characteristics are given in Table II.[9]

2.B. MRI sequence for tumor diagnosis, segmentation, and treatment planning

Each canine patient was scanned in a 1.5-T Phillips Intera magnet according to the standardized clinical brain tumor protocol sequences presented in Table I. Mimics 14.1 image analysis software (Materialise, Leuven, Belgium) and the Visifield (www.visifield.com) software were used to segment the normal brain and tumor tissue in the T1-weighted post-contrast MRI sequences. The tumors were traced in a semi-automated manner in each of the two-dimensional (2-D) axial planes based on the increased intensity due to Gadolinium uptake. The treatment zones were identified by (a) the changes of Gadolinium contrast agents in T1W + C scans or (b) anatomical inspection of the tumor location in the two canine patients with non-enhancing tumors. Specifically, therapeutic response assessments were evaluated with response assessment in neurooncology (RANO) criteria.[35] For each patient individually, the segmented medical images were used to construct the 3D model using the following approach. The electrode tips and trajectories were identified in the original medical images. The electrodes were then inserted in the model as cylinders with 1-mm diameter and length according to the case, while aligning the coordinate system of the model with that of the original medical images. The mesh was built in a rectangular cuboid domain with the faces either 5 cm away from the electrodes or corresponding to the edges of the original medical images, whichever was closer. For the investigation of the effect of increasing or reducing the tumor size, the binary segmentation image was dilated or eroded with a circular structural element with a radius of two pixels in the axial slices. The tumor was not dilated or eroded in the z direction of the images, because the distance between slices was much larger than the pixel size and some tumors were visible only for a few sequential slices (e.g., three slices in the case of patient 3). Although the electrodes displaced a small volume of tissue during the treatment, the model was not deformed in any way because the tissue was soft and compressible.

2.C. Computational modeling of electric field for assessing tumor coverage

The electric field modeling was performed using the finite element method. We used COMSOL Multiphysics (Comsol AB, Stockholm, Sweden) and its AC/DC module to model the electric field. The stationary Laplace equation for electric potential was solved in the box-shaped computational domain, which extended 5 cm from the outer dimensions of the electrodes. The active electrodes were assigned the Dirichlet boundary condition, while the outer boundaries were defined as electrically insulating. The electric field was solved with an iterative scheme, where COMSOL Multiphysics was controlled from Matlab (Mathworks, Natick, MA, USA). The material properties were assigned to the mesh elements according to the segmented images, where each tissue was assigned different electrical properties.[36] The electric properties of tumor and brain tissues were taken from previous work,[28,30] since the increase of conductivity during electroporation is a well-documented phenomenon.[37,38] The values of tissue conductivities used are reported in Table III.[39,40] Each iteration consisted of a static simulation

TABLE I. Sequence parameters for MRI acquisition in canine patients.

Sequence	Image weighting	Acquisition plane	2D vs. 3D	TE (ms)	TR (ms)	TI (ms)	Flip angle (degrees)	NEX	Echo train length	Slice thickness (mm)	Interslice gap (mm)	FOV (mm)	Matrix dimensions	b-value
TSE	T2	Sag.	2D	100	3828	–	90	6	15	3	3.3	110	184 × 179	–
TSE	T2	Trans.	2D	110	7048	–	90	6	22	3	3.3	110	184 × 158	–
GRE	T2	Trans.	2D	23	1050	–	18	2	1	3	3.3	110	156 × 142	–
SE	T1	Trans.	2D	11	400	–	80	2	1	2.6	2.9	110	184 × 201	–
SE	T1	Sag.	2D	11	400	–	80	2	1	3	3.3	110	184 × 183	–
GRE	T1	Trans.	3D	4.5	25	–	30	2	1	1.6	0.8	110	168 × 167	–
FLAIR	T2	Trans.	2D	140	11000	2800	90	4	27	3	3.3	110	140 × 90	–
DWI	T2	Trans.	2D	72	4216	–	90	3	63	2.6	2.9	110	72 × 57	1000
S/G/D[a]	T2	Trans.	3D	49	35	–	7	1	19	3.5	–	110	64 × 60	–
SE	T1 Post	Trans.	2D	11	400	–	80	2	1	2.6	3.3	110	184 × 201	–
SE	T1 Post	Sag.	2D	11	400	–	80	2	1	3	3.3	110	184 × 183	–
SE	T1 Post	Dorsal	2D	11	400	–	80	2	1	3	3.3	110	216 × 185	–
GRE	T1 Post	Trans.	3D	4.5	25	–	30	2	1	1.6	0.8	110	168 × 167	–

[a]Denotes S-PRESTO/GRE/DCE-MR.

TABLE II. Physical tumor characteristics, electrode configuration, and electrical parameters employed during irreversible electroporation treatment of spontaneous malignant glioma.

Patient	Tumor type	Tumor (cm^3)	Electrode number	Pulses per electrode pair	Total pulses	Voltage (V)	Post-IRE (months)	Best clinical outcome
1	AOA	1.15	2	40/80	120	500/625	4	CR
2	GBM	2.85	2	80/80	160	625/500	n/a	ND
3	AO	0.98	4	80/80	160	750/1000	3	PR
4	AA	2.17	6	90/90/90	270	900/1000/800	24[a]	CR
5	GBM	4.98	6	50/50/50	150	500/1000/1000	2	PR
6	O	0.55	2	90	90	1000	12	SD
7	A	0.85	4	40/40/40/40	160	800/800/800/800	2	SD

Note: [a]This patient has been in complete response for 5+ years post-IRE treatment. AA, anaplastic (Grade III) astrocytoma; AO, anaplastic (Grade III) oligodendroglioma; AOA, anaplastic (Grade III) oligoastrocytoma; GBM, glioblastoma multiforme (Grade IV astrocytoma); O, Grade II oligodendroglioma (Grade II); A, astrocytoma (Grade II).

TABLE III. Physical tissue properties employed in the treatment planning models.

Tissue	$\sigma_{initial}$ (S/m)	σ_{maxium} (S/m)	References
Gray matter	0.285	0.7359	[39]
White matter	0.3621	0.7357	[39]
Brain tumor (glioma)	0.435	0.7373	[39]
Skull	0.02	n/a	[40]

of the electric field; however, between the iterations, the tissue conductivities were increased as a function of the electric field.[30,41,42] This was repeated for every electrode pair used in the treatment and the maximum electric field was recorded.[43] For the outcome analysis, the maximum electric field from all electrode pairs was taken to compute the coverage of the treated volume.

2.D. Cell kill probability calculations for patient-specific brain tumors

The modeling of cell kill probability was performed using the Peleg-Fermi model.[44] This mathematical description was first developed to describe microbial inactivation after treatment with pulsed electric fields, and later adapted for use in irreversible electroporation.[31–33] The model uses the following equation:

$$S = \frac{1}{1 + exp\left[\frac{E - E_c(n)}{A(n)}\right]}, \quad (1)$$

where S is the probability of cell survival, E is the electric field to which the cells are exposed, $E_c(n)$ is the critical electric field as a function of the number of pulses over which 50% of cells are expected to die and $A(n)$ is a shape factor which determines the transition between unaffected and completely ablated tissue. Specifically, $E_c(n)$ and $A(n)$ are defined as follows:

$$E_c(n) = E_{c0} \cdot exp(-k_1 n), \quad (2)$$

$$A(n) = A_0 \cdot \exp(-k_2 n), \quad (3)$$

with E_{c0} being the initial value of the critical electric field, A_0 the initial value of the shape factor, k_1 and k_2 the exponential decay coefficients, and n being the number of pulses used in the treatment respectively. Although the model was initially based on *in vitro* data, it has since been applied to *in vivo* results for IRE in normal brain tissue of rats.[45] The values of the parameters used in the literature so far are listed in Table IV. The exact values of parameters were adjusted from Sharabi et al.[45] based on the complete response (CR) achieved in patient 4 with IRE treatment alone.

In the cases where more than one electrode pair was used, Eq. (1) was computed for every electrode pair separately as a scalar field and then multiplied:

$$S(x, y, z) = \prod_{\forall i} S_i(x, y, z) \quad (4)$$

where S_i is the probability of survival for i-th electrode pair. The cell kill probability is then defined as $1 - S$.

3. RESULTS

3.A. Electric field distribution within MRI-based intracranial environment

One of the main advantages of IRE in comparison with other focal ablation techniques is the dependency on the electric field exposure to achieve therapeutic effects. Sufficient electric field exposure is thus required for tumor response to the IRE treatment without damaging surrounding critical structures such as major blood vessels. The steps to compute the electric field distribution from MRI-based volumetric reconstructions of the tissue and tumor components in the brain are demonstrated in Fig. 1. First, individual tissues (e.g., white matter, gray matter, and tumor) are segmented from each of the MR images in the sequence [Fig. 1(a)]. The tissue-specific segmentation allows for determining the tumor dimension and formulating the insertion approach to use during the surgery. The individual 2D segmentations are then reconstructed to generate a single 3D volumetric representation of the tissue components [Fig. 1(b)]. The volumetric

representation allows for the virtual placement of the electrode geometry within or around the target tumor. The electrodes employed during the IRE treatment are insulated in order to protect the normal brain tissue outside of the 5-mm active electrode tips [Fig. 1(c)]. Finally, the 3D volumetric reconstructions are meshed to allow for computational simulations of the physical effects of the electric pulses. Figure 1(d) shows the electric field distribution within the tumor (red mesh) that is generated by a 4-electrode array. We demonstrated that therapeutic IRE planning is possible for patients with deep-seated tumors using anatomically accurate computational models to prevent damage to critical structures surrounding the zone of ablation.

3.B. Numerically simulated tumor exposure to electric field

The computational models were used to define the electrode configuration and electric pulse parameters for the intraoperative IRE treatments with the goal of maximizing tumor coverage while minimizing damage to the surrounding healthy tissue.[46] Figure 2 presents results that replicate the intraoperative electrode configuration, surgical placement, and electrical parameters employed during the IRE treatments (Table I). The patient-specific curves in the plot illustrate the electric field coverage normalized to the tumor dimensions. In all patients, decreasing the electric field threshold for cell kill results in a higher tumor fraction. Patient 6 for example demonstrates ~ 60% tumor coverage with ≥ 600 V/cm. The tumor coverage in this same patient increases to ~ 95% when the threshold is reduced to ≥ 300 V/cm. The computational models are thus relevant since they provide IRE treatment insight to the tumor fraction exposed to a known lethal electric field magnitude. The lethal electric field threshold is specific to the treatment parameters used, so implementing an algorithm that accounts for other variables such as pulse number and pulse duration would further improve the robustness of the computational models.[47]

TABLE IV. Values of the Peleg-Fermi model parameters in the literature.

Reference	Model	E_{c0} (V/cm)	A_0 (V/cm)	k_1	k_2
Goldberg et al.[31]	CHO cells	4,000	1,441	0.03	0.06
Dermol et al.[33]	CHO cells	2,734	326	0.025	0.0016
Sharabi et al.[45]	Rat brain	1,062	11	0.007	0.002
Peleg[44]	*Pseudomonas aeruginosa*	12,200	2,500	0.024	0.012

3.C. Statistical cell kill model allows incorporation of pulse number and pulse duration

In order to more accurately recapitulate the effects that occurred during the IRE treatments of the canine patients, the computational models were refined to include parameters such as pulse number and pulse duration. Figure 3 displays the probabilities of cell kill due to electric field exposure as computed from the Peleg-Fermi model. The values of the parameters for the Peleg Fermi model for gliomas were also targets of

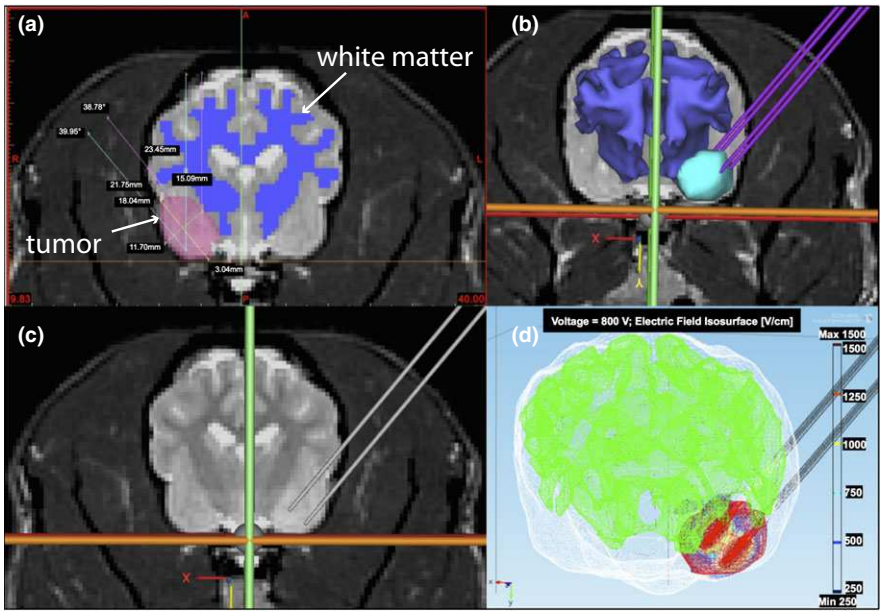

FIG. 1. MRI-based planning of irreversible electroporation (IRE) treatment of malignant glioma in canine patients. (a) White matter and tumor segmentation and corresponding measurements (e.g., distance and angles) for electrode placement. (b) 3D volumetric reconstruction of the gray matter, white matter, and tumor tissue from MR images and the corresponding electrode geometry used during surgical procedures. (c) Planned electrode insertion depth and trajectory for delivering intratumoral pulsed electric fields. (d) Computational simulation of the electric field distribution surrounding the active electrodes during pulse delivery in order to compute tumor coverage and cell kill probabilities. Panels (a)–(d) were developed with MRI data from patient 7 (Table II). [Color figure can be viewed at wileyonlinelibrary.com]

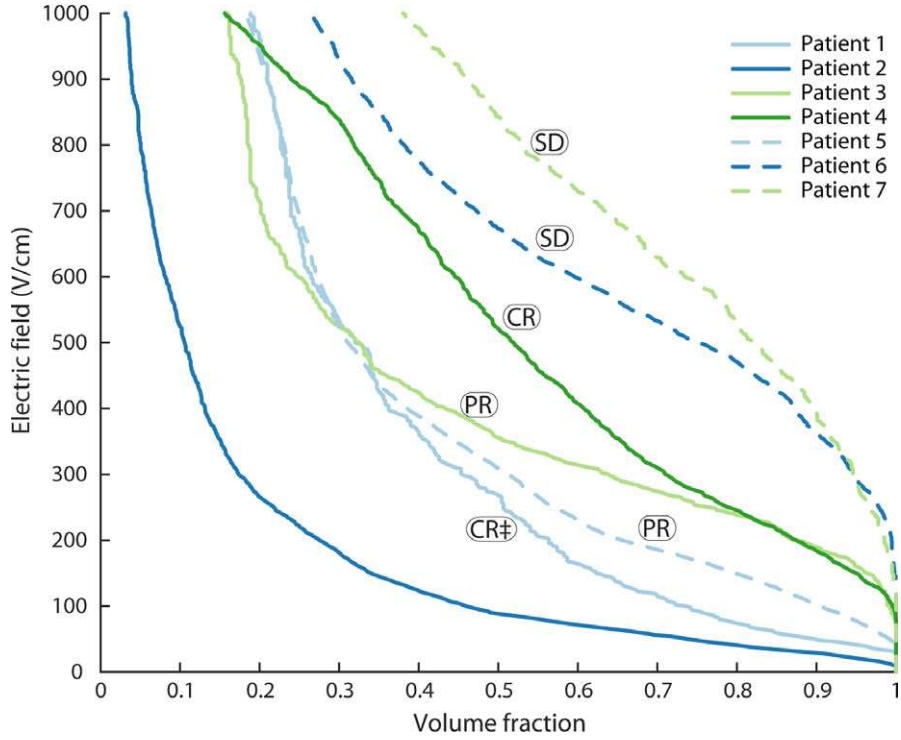

FIG. 2. Tumor coverage during the IRE treatment of spontaneous glioma. The seven canine patients with brain cancer were treated with parameters shown in Table I. The tumor fraction was computed as a function the electric field exposure and is normalized by the tumor dimension. This model demonstrates good correlation with radiographically confirmed clinical outcomes but lacks important information on treatment parameters such as pulse number and pulse duration. Note: Patient 1 resulted in complete response with IRE and adjuvant fractionated radiotherapy (denoted by ‡) but developed treatment-related brain necrosis and leukoencephalopathy confirmed at necropsy without signs of recurrent malignant glioma.[10] [Color figure can be viewed at wileyonlinelibrary.com]

this investigation. We used Peleg-Fermi parameter values based on Sharabi et al.[45] where the narrow transition region between IRE-ablated and unablated regions was also noted. The values for A_0, E_{c0}, and the exponent scaling factors k_1 and k_2 were adjusted from *in vivo data* for normal rat brain to accommodate the output of the model with the radiologically confirmed clinical outcomes. Three distinct regions can be visualized in the contour plot that results in very different therapeutic outcomes (Fig. 3). If the electric field is not strong enough or if not enough pulses are delivered, there is no therapeutic effect (dark blue zone). Conversely, if the electric field is too strong or an excessive number of pulses is delivered, the cells are killed by IRE with or without thermal damage in the immediate vicinity of the electrodes (yellow zone).[32] Finally, there is also a transition zone that demonstrates that ≥ 80 pulses are necessary to achieve high probabilities of cell kill at relatively mild (~ 300 V/cm) electric field strengths. The Peleg-Fermi model increases the predictive power of our MRI-based computational models since it is capable of discriminating the tumor coverage between patients that were treated with the same electric field distribution but differ in pulse number for example.

3.D. Relationship between numerically predicted tumor coverage with radiographically confirmed clinical outcome

Figure 4 shows the simulated probability of cell kill as a function of the volume fraction of the tumor for the seven canine patients treated in this study. These MRI-based computational models recapitulate the 3D tumor and brain reconstructions, electrode placement, and pulse parameters employed during the IRE treatments (Table I). In four of the five canine patients (Patients # 3, 4, 6, 7) treated with curative intent, the tumor fraction was ≥ 0.9 for a cell kill probability $\geq 90\%$. These patients resulted in a complete response (Patient # 4), stable disease (Patients # 6 and 7), and partial response (Patient # 3) based on MRI-evaluation post-IRE. Even though canine patient 1 exhibited a lower cell kill probability, the IRE treatment alone resulted in a radiographically confirmed 75% tumor reduction 3 days post-treatment and was in complete response at 4 months (with adjuvant radiation therapy).[10] As expected, patients # 2 and # 5 that were treated with the palliative intent of reducing the burden from their oversize tumors resulted in the lowest tumor coverage. Our results confirm that these models are capable of predicting radiographically confirmed clinical outcomes and can be used to evaluate the appropriate number of pulses to use in a clinical setting. For clinical reasons unrelated to this study, patient 7 was euthanized 3 months post-IRE treatment and was confirmed to be tumor-free on postmortem examination. Thus, the data suggest that a tumor coverage of ≥ 0.9 at a cell kill probability $\geq 90\%$ can be safely used to guide IRE treatments.

Figures 5 and 6 demonstrate the predictive power of the cell kill probability in comparison with the tumor coverage with electric field alone. Specifically, Fig. 5 depicts canine

patient # 4 in which a complete response was achieved at 3 months [Fig. 5(d)], 12 months [Fig. 5(e)], and 18 months [Fig. 5(f)]. This patient has been in complete response for 5+ years post-IRE treatment. Figure 6 depicts the scenario in which a partial response was detected at 2-weeks [Fig. 6(d)] and 2 months [Fig. 6(e)] post-IRE. Additionally, it provides a comparison between the tumor coverage achieved with the electric field alone [Fig. 6(a)] and cell kill probability [Fig. 6(b)] modeling approaches. More importantly, as is evident from the progressive disease (PD) detected at 4 months [Fig. 6(e)] could be considered as incomplete treatment as regrowth seems to have originated from the untreated portion of the tumor depicted in red in Figs. 6(a) and 6(b).

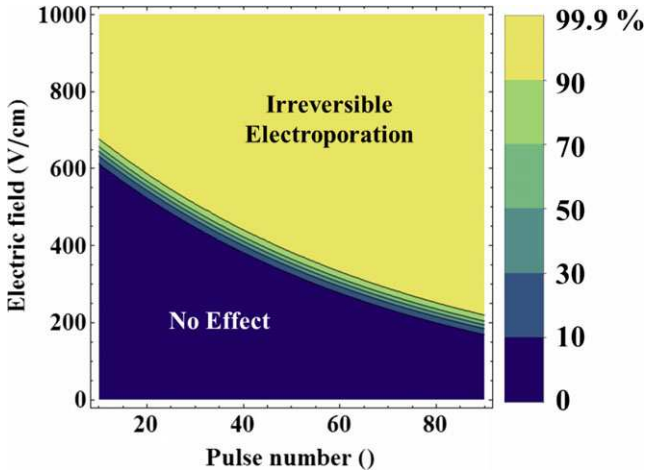

FIG. 3. Peleg-Fermi cell kill probability during pulsed electric field exposure. The cell kill probability distribution is given as a function of electric field and pulse number with the following parameters (E_{c0} = 750 V/cm, A_0 = 15 V/cm, k_1 = 0.015, k_2 = 0.003). The three distinct regions represent no effect, a transition zone, and complete cell kill due to irreversible electroporation. Delivering more pulses at a specific electric field can increase the cell kill probability. Similarly, one can generate a higher probability of cell kill by increasing the electric field at a specific pulse number. [Color figure can be viewed at wileyonlinelibrary.com]

3.E. Cell kill probability in dilated and eroded tumor geometries

In order to illustrate the robustness of the 3D volumetric reconstructions of the tumor geometries, dilated and constricted versions of the reconstructions were also created. Figure 7 shows the tumor-to-tumor variability that could be introduced if the MRI-based reconstructions are artificially manipulated. The variability in the cell kill probability depends on the tumor volume, electric field distribution, and pulse number as expected. The largest variability was seen in patients # 1 (small tumor), 3 (small tumor), and 7 (low pulse number). On the other hand, patients # 2 (large tumor), 5 (large tumor), and 6 (high pulse number) demonstrate less variability. The volume fraction of tumor coverage (solid black lines) is perhaps a better indicator of the

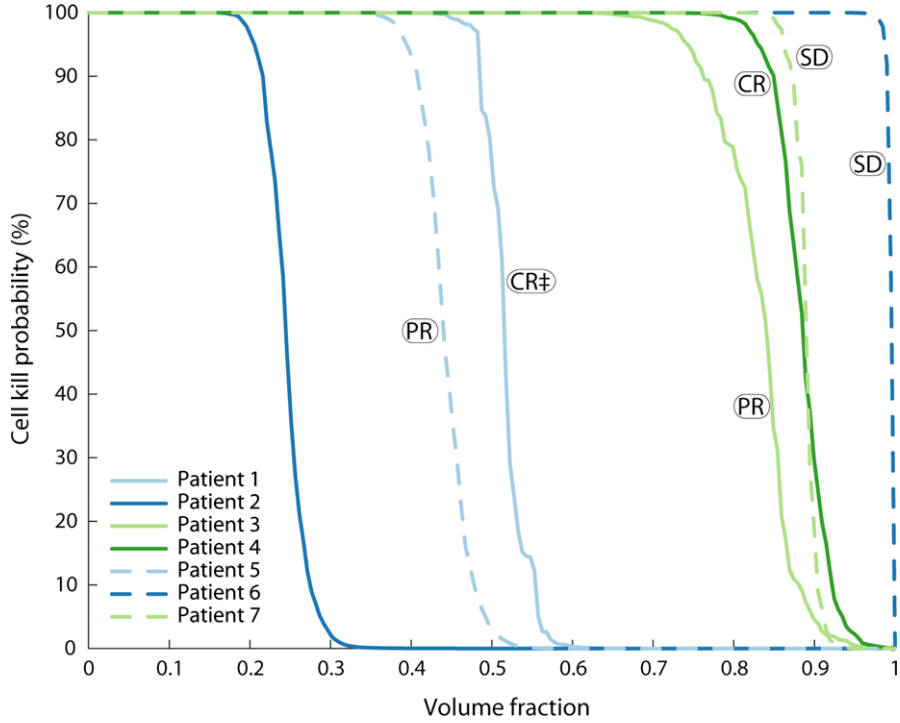

FIG. 4. Statistical model of cell kill during the irreversible electroporation treatment of spontaneous glioma. The seven canine patients with brain cancer were treated with parameters shown in Table I. The cell kill probability was computed as a function the tumor fraction. This statistical model correlates well with radiographically confirmed clinical outcomes and incorporate the pulse number and pulse duration employed during the treatment. The patients that responded best to IRE therapy demonstrated tumor coverage ≥ 0.9 at a cell kill probability ≥ 90%. Patient # 7 was treated with 40 pulses for each of the two electrode pairs and resulted in radiographically confirmed stable disease and was confirmed to be tumor-free on post-mortem examination. Note: Patient 1 resulted in complete response with IRE and adjuvant fractionated radiotherapy (denoted by ‡) but developed treatment-related brain necrosis and leukoencephalopathy confirmed at necropsy without signs of recurrent malignant glioma.[10] [Color figure can be viewed at wileyonlinelibrary.com]

radiographically confirmed clinical outcome since patients with tumor coverage ≥ 0.5 at a cell kill probability ≥ 50% resulted in substantial improvements after the IRE treatment and resulted in complete response (Patients # 1 and 4), partial response (Patients # 3 and 5), and stable disease (patients # 6 and 7). The capability of using these predictive tools for planning IRE procedures will further improve the clinical outcomes of these malignant glioma patients.

3.F. Radiographically confirmed clinical outcomes and KPS evaluation post-IRE

Figure 8 demonstrates that all the patients that were treated with curative intent benefited from the IRE procedure. Data is unavailable for patient 2 since it developed fatal (Grade 5) aspiration pneumonia within 14 days of the cytoreductive IRE treatment. These radiographically confirmed clinical outcomes are demonstrated in the complete responses (patients 1 and 4), partial responses (patients 3 and 5), and stable disease (patients 6 and 7) achieved in the clinical trial. Additionally, the imaging-based IRE treatment extended the survival of several patients past the 1-month survival without treatment reported in other studies.[5] Finally, in order to assess the quality of life of our patients, the Karnosky Performance Score (KPS) was evaluated and resulted in improvements in every canine patient. This demonstrates the ability of a one-time treatment to generate lasting positive results in tumor control and quality of life.

4. DISCUSSION

The safety and potential for using pulsed electric fields for therapeutic brain applications has been demonstrated in animal models[18,48–50] and canine patients with spontaneous

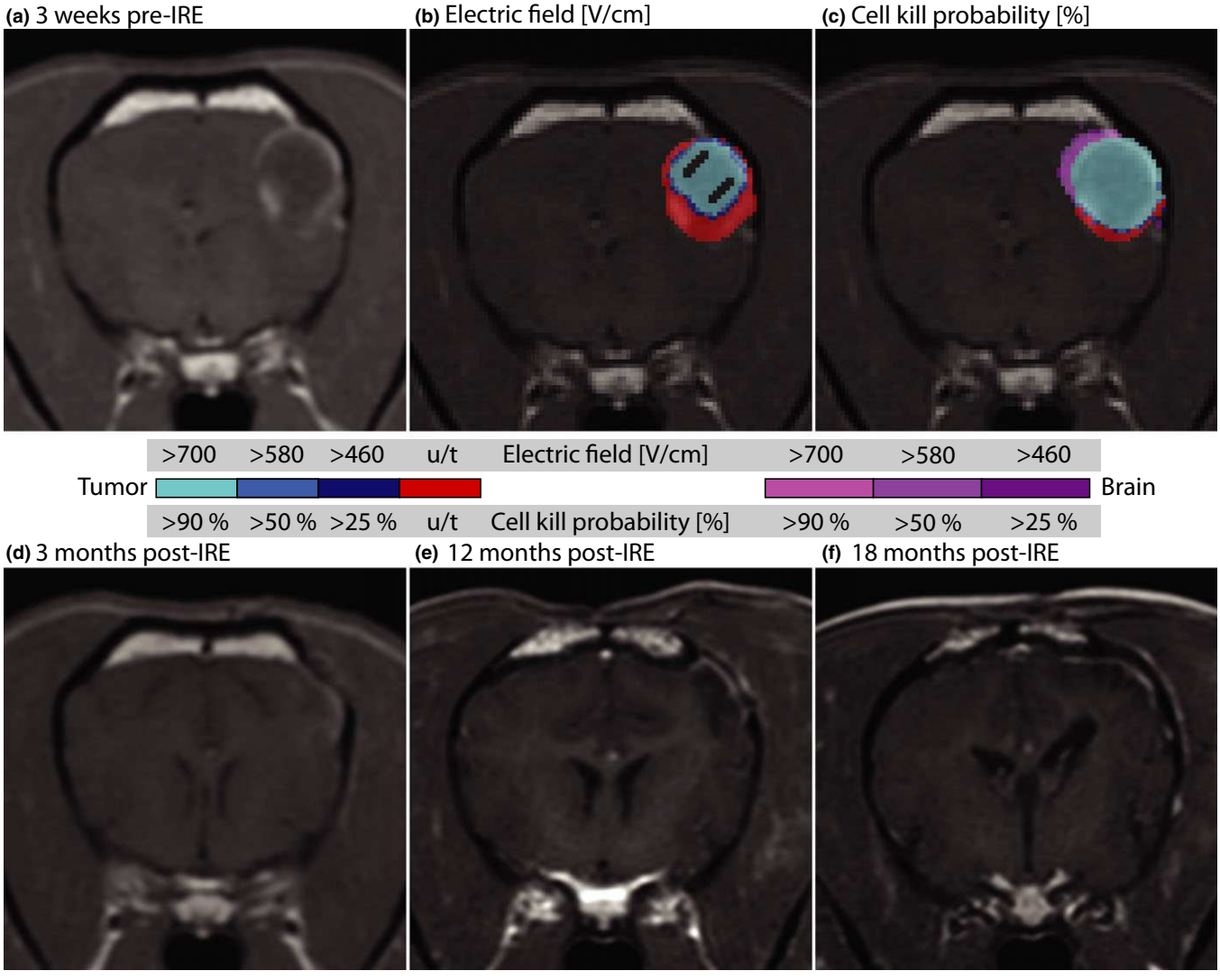

FIG. 5. Imaging before and after IRE treatment in patient # 4. The patient was diagnosed (a) 3 weeks prior to receiving IRE therapy based on clinical and radiological MRI evaluation. Tumor and brain tissue coverage computed from the (b) electric field distribution and with (c) the Peleg-Fermi cell kill model. The patient was found to be in complete response (CR) at (d) 3 months, (e) 12 months, and (f) 18 months post-IRE based on radiological MRI evaluation. This patient has been in complete response for 5+ years post-IRE. u/t denotes untreated tumor tissue. [Color figure can be viewed at wileyonlinelibrary.com]

disease.[9,10] These applications involve reversible disruption of the blood-brain-barrier for delivery of therapeutic agents[48,49,51,52] or irreversible treatment for localized tissue/tumor ablation.[9,10,53] Recently, Tumor Treating Fields (TTFs) received FDA approval for GBM treatment due to the demonstrated ability to add 3 months to the progression-free and overall survival of human patients when used in combination with temozolomide chemotherapy in a phase III clinical trial.[54] Despite encouraging clinical outcomes, the median survival for human GBM patients is only 15 months with singular or multimodal therapy consisting of surgical resection, chemotherapy, and/or radiation therapy.[1,2] In this study, all the canine patients that were treated with curative intent demonstrated partial-to-complete responses and improved quality of life, including a patient (patient 4) that has been tumor free for 5+ years and one that was tumor free based on histological evaluation post-mortem 3 months after treatment.

Brain tumor coverage with sufficiently strong electric field is a requirement for positive tumor control.[26] In previous *in vivo* work, an electric field of ~500 V/cm has been reported as the electric field threshold for normal brain tissue ablation using fifty 70-μs pulses at 4 Hz in rats[50] or ninety 50-μs pulses at 4 Hz in dogs.[28] However, from the tumor coverage simulations shown in Fig. 2 (electric field) and Fig. 4 (cell kill probabilities) it appears that canine patient # 4 only reached ~ 0.95 volume fraction at 50% cell kill probability. This suggests that there is additional therapeutic assistance in order to achieve the 5+ years complete response observed in this canine patient. Specifically, recent IRE studies suggest

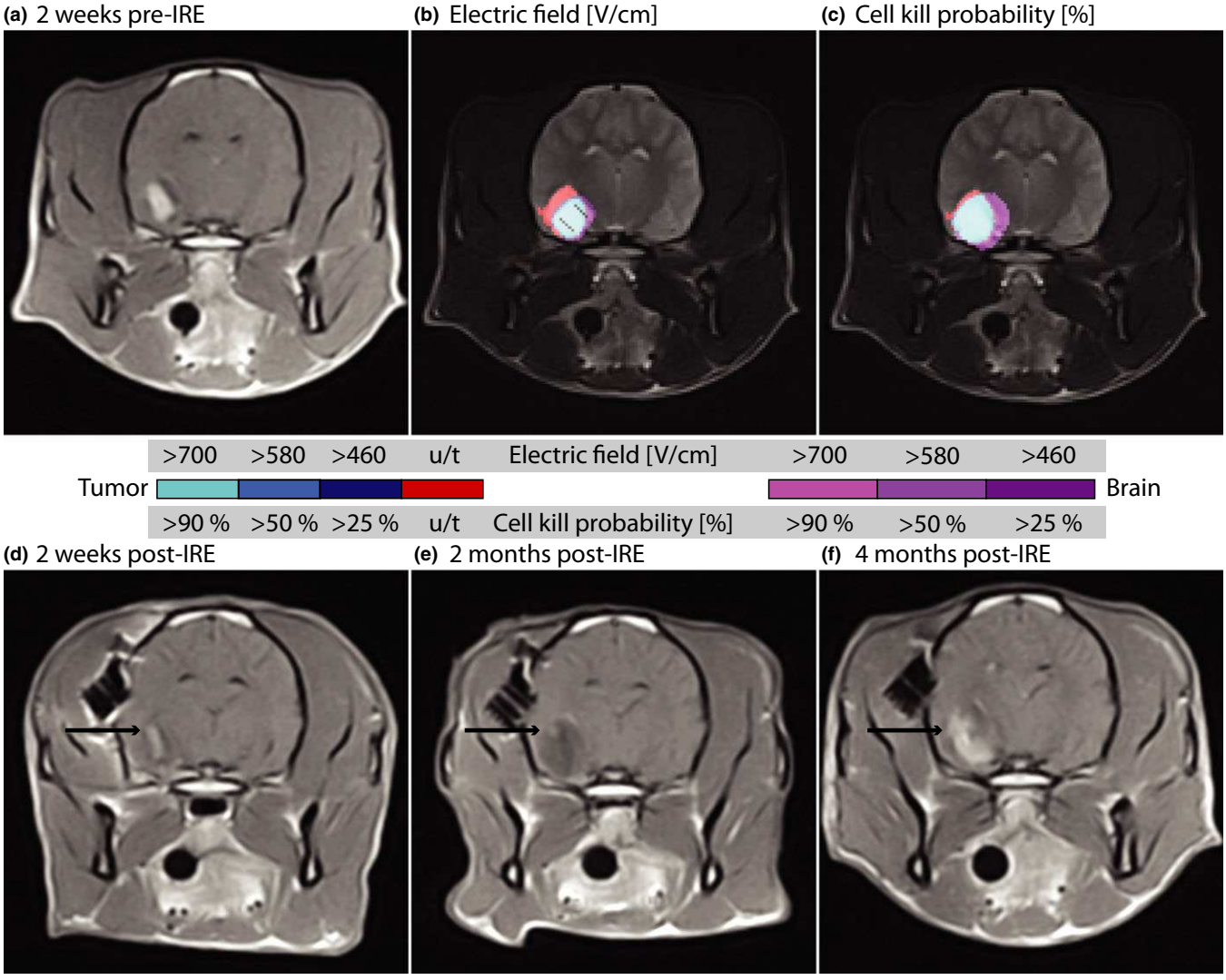

FIG. 6. Imaging before and after IRE treatment in patient # 3. The patient was diagnosed (a) 2 weeks prior to receiving IRE therapy based on clinical and radiological MRI evaluation. Tumor and brain tissue coverage as computed from the (b) electric field distribution and with (c) the Peleg-Fermi cell kill model. The patient was found to be in partial response (PR) at (d) 2 weeks with the arrow indicating remnants of the tumor, which is further resolved at (e) 2 months post-IRE, with only a small viable region remaining. (f) Subsequent progressive disease (PD) 4 months post-IRE with the tumor growth located in the previously untreated region. The location of the recurrence is consistent with the untreated portion of the tumor as indicated by u/t coloring in (b) and (c). [Color figure can be viewed at wileyonlinelibrary.com]

that there might be an immune response that is triggered with the nonthermal ablation and may help in tumor control.[55,56] Despite promising results, there are limited studies evaluating the IRE-induced immune response and there is a need for additional studies that include combinatorial therapies as well.[57]

The limitations of the current study lie in the heterogeneity of the patient population and the tumor types and locations.

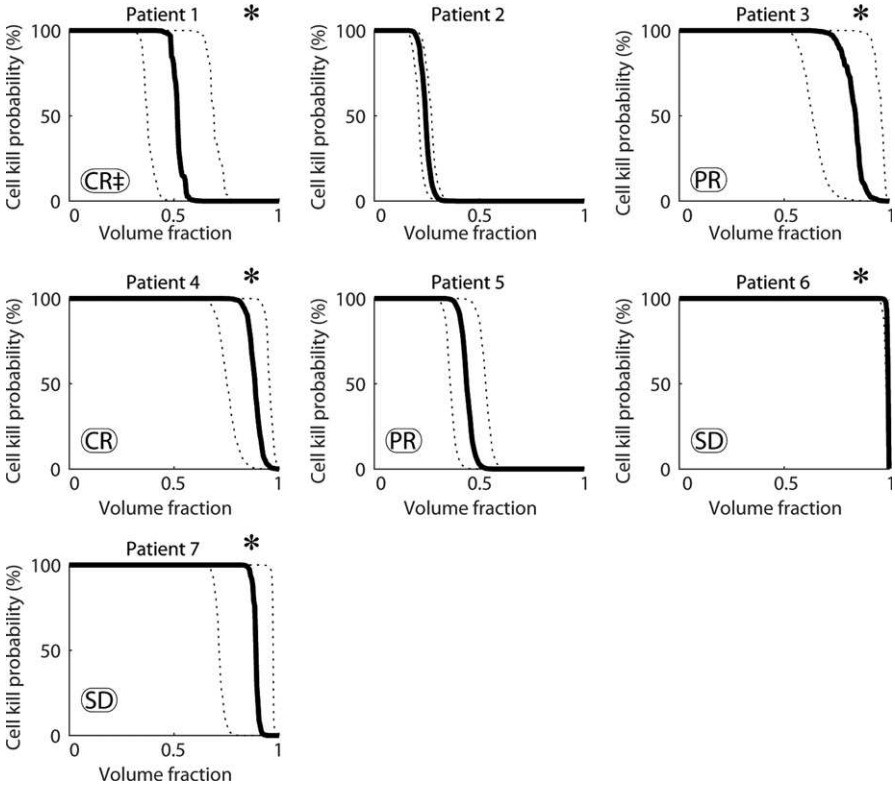

FIG. 7. Evaluation of cell kill distributions based on dilated and constricted 3D volumetric tumor reconstructions. The volume fraction is directly correlated with the radiographically confirmed clinical outcome since patients with volume fraction ≥ 0.5 at a cell kill probability ≥ 50% resulted in substantial improvements compared to those with volume fraction ≥ 0.5 at a cell kill probability < 50%. *Denotes the patients that were treated with curative intent. Note: Patient 1 resulted in complete response with IRE and adjuvant fractionated radiotherapy (denoted by ‡) but developed treatment-related brain necrosis and leukoencephalopathy confirmed at necropsy without signs of recurrent malignant glioma.[10]

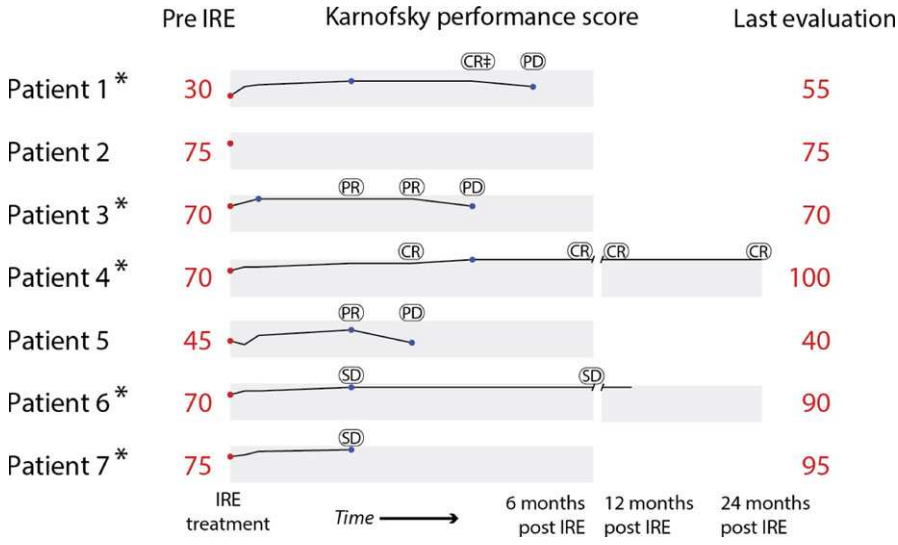

FIG. 8. Radiographically confirmed clinical outcomes and Karnosky Performance Score (KPS) evaluation pre- and post-IRE treatment. The KPS scores demonstrate that all treatments with curative intent resulted in substantial improvement post-IRE. Additionally, the IRE treatments achieved two complete responses, three partial responses, and two stable disease. * Denotes the patients that were treated with curative intent. [Color figure can be viewed at wileyonlinelibrary.com]

The seven patients are from different types of dog breeds which means a large variability in the genetic factors and possibly differences in the capabilities of the immune system. There were also histological differences between tumors in the patient population. The tumor sizes were also very diverse, with the smallest being 0.5 cm^3 and the largest 5.0 cm^3. Another limitation is the transition from *in vitro* models that were used to develop the statistical approach for cell survival. Namely, the first proposal to use the Peleg-Fermi model was based on *in vitro* studies of cell killing with up to 10 pulses.[31] A more recent study concluded that the mathematical description used in this model is accurate, however, using a larger number of pulses resulted in substantially different parameters of the model.[33] This model has also been used to evaluate cell death of normal brain tissue,[45] but not yet for brain tumors. The parameters of the Peleg-Fermi model found in this study can therefore be considered to be based on *in vivo* data and glioma-specific, but additional experiments need to be performed to determine if the tumor grade at treatment has an effect on the model parameters. It is likely that specific parameters of the cell death model may need to be found for each different tumor histological type. Another limitation is that the current model does not take into account the action of the immune system, therefore it could lead to using overly aggressive pulse protocols when attempting to ensure 99.99% cell death in the entire radiologically confirmed tumor volume.

The clinical implementation of the presented study will be possible in the near future. The required steps would be additional studies for determination of the safety of such a treatment in human patients with malignant glioma. A treatment planning framework similar to the approach used in radiotherapy is already in development (Visifield.com), but was used in this study only for segmentation of the brain and tumor tissue for patients 1 and 2. Initially, treatment planning has been envisioned as being performed in advance of the treatment, i.e., at least a day or up to a week before. This can be performed on contemporary personal workstation computer, since the determination of the electric field between one pair of electrodes takes approximately 3 min. In order to perform treatment planning during the treatment itself – based on actual realized positioning of the electrodes, the time of computation however would need to be reduced considerably. With image fusion with intraoperative imaging, this kind of approach may also allow for inclusion of tissue deformations due to electrode insertion, which were not considered in this study. In the case of treatment of brain tumors, careful positioning of the electrodes and planning of the clinical target volume is critical. The feasibility of using numerical treatment planning for brain tumors has been studied previously[25] and validated in this study using real clinical cases and confirmed using radiological evaluation post-treatment. The treatment planning approach and optimization of the cases has been developed previously[21,58] and is extended in the current study using statistical modeling of the treatment outcome. The coupling of such a treatment planning approach with existing solutions for optical navigation has also been demonstrated.[22,59] Therefore, each step in the treatment workflow has been developed. The translation into the clinic would therefore only require the combination of the already developed steps into a finalized multidisciplinary approach. Before implementation into clinical practice, it is still necessary to obtain regulatory approval, since any kind of treatment planning tool for delivery of energy has to be considered as a medical device.

For direct and immediate prediction of the treatment outcome, the monitoring of electric field during the treatment using MRI has been demonstrated on a research magnet.[60,61] Using this approach, the electric field and the expected outcome of the treatment can be known immediately after the end of electroporation pulse delivery, potentially identifying any areas where the expected treatment efficacy could be suboptimal. To realize this monitoring, further steps are required: the development of MRI compatible electrodes and pulse generator, validation of the method in a clinical scanner, and validation of the predicted outcomes with clinical data.

5. CONCLUSIONS

This study presents the first attempt to validate numerical models of cell death in a spontaneous tumor tissue. The treatment protocols used during the surgical procedures of the canine patients allowed us to fine-tune the computational models and establish their predictive power for use in therapeutic IRE planning. We conclude that for the chosen parameters of the Peleg-Fermi models, a coverage of more than 0.9 volume fraction of the tumor with more than 90% probability of cell kill is a good predictor of therapeutic success. The parameters of the Peleg-Fermi model are also such that they require lower electric fields to achieve success than are typically used in IRE procedures. This will be very useful in cases where sparing critical structures is essential for the treatment safety and/or maintaining patients' quality of life. Finally, the electric field thresholds that produced good treatment outcomes were also lower than commonly reported in the IRE literature outside the brain.

ACKNOWLEDGMENTS

This work was supported by the Wallace H. Coulter Foundation Early Career Translational Research Awards and the National Science Foundation CBET-0933335 and CAREER CBET-1055913. This research was supported in part by the Slovenian Research Agency (Grants BI-US/14-15-016, P2-0249 and Z3-7126). It has been performed within the scope of LEA EBAM. The study was made possible due to networking efforts of the COST TD1104 action (www.electroporation.net). AngioDynamics, Inc. loaned the NanoKnife System and manufactured the electrodes used in the study (www.angiodynamics.com).

AUTHOR CONTRIBUTIONS

Conceived and designed the simulations: PAG BK DM RVD. Performed the canine treatments: JHR PAG RVD.

Analyzed the data: PAG BK JHR RVD DM. Contributed materials/analysis tools: DP DM RVD. Wrote the paper: PAG BK JHR DM RVD.

CONFLICTS OF INTEREST

BK and DP have no competing interests. PAG, RVD, and JHR have pending and issued patents in the area of irreversible electroporation. RVD has also provided consulting services to AngioDynamics and received travel reimbursement for company meetings. DM holds patents on electrochemotherapy that have been licensed to IGEA S.p.a. and is also consultant to various companies with interest in electroporation based technologies and treatments.

*These authors contributed equally to this work.
[a)]Author to whom correspondence should be addressed. Electronic mail: pagarcia@mit.edu.

REFERENCES

1. Stupp R, Mason WP, van den Bent MJ, et al. Radiotherapy plus concomitant and adjuvant temozolomide for glioblastoma. *N Engl J Med*. 2005;352:987–996
2. La Rocca RV, Mehdorn HM. Localized BCNU chemotherapy and the multimodal management of malignant glioma. *Curr Med Res Opin*. 2009;25:149–160
3. Chen L, Zhang Y, Yang J, Hagan JP, Li M. Vertebrate animal models of glioma: understanding the mechanisms and developing new therapies. *Biochim Biophys Acta (BBA)*. 2013;1836:158–165.
4. Kimmelman J, Nalbantoglu J. Faithful companions: a proposal for neurooncology trials in pet dogs. *Cancer Res*. 2007;67:4541–4544.
5. Heidner GL, Kornegay JN, Page RL, Dodge RK, Thrall DE. Analysis of survival in a retrospective study of 86 dogs with brain tumors. *J Vet Intern Med*. 1991;5:219–226
6. Stoica G, Kim HT, Hall DG, Coates JR. Morphology, immunohistochemistry, and genetic alterations in dog astrocytomas. *Vet Pathol*. 2004;41:10–19
7. Dickinson PJ, LeCouteur RA, Higgins RJ, et al. Canine spontaneous glioma: a translational model system for convection-enhanced delivery. *Neuro Oncol*. 2010;12:928–940.
8. Pluhar GE, Grogan PG, Seiler C, et al. Anti-tumor immune response correlates with neurological symptoms in a dog with spontaneous astrocytoma treated by gene and vaccine therapy. *Vaccine*. 2010;28:3371–3378.
9. Rossmeisl JH, Garcia PA, Robertson JL, et al. Safety and feasibility of the NanoKnife system for irreversible electroporation ablative treatment of canine spontaneous intracranial gliomas. *J Neurosurg*. 2015;123:1008–1025.
10. Garcia PA, Pancotto T, Rossmeisl JH, et al. Non-thermal irreversible electroporation (N-TIRE) and adjuvant fractionated radiotherapeutic multimodal therapy for intracranial malignant glioma in a canine patient. *Technol Cancer Res Treat*. 2011;10:73–83.
11. Cannon R, Ellis S, Hayes D, Narayanan G, Martin RC 2nd. Safety and early efficacy of irreversible electroporation for hepatic tumors in proximity to vital structures. *J Surg Oncol*. 2013;107:544–549.
12. Deipolyi AR, Golberg A, Yarmush ML, Arellano RS, Oklu R. Irreversible electroporation: the evolution of a laboratory technique to be used in interventional oncology. *Diagn Interv Radiol*. 2014;20:147–154.
13. Martin RC 2nd, McFarland K, Ellis S, Velanovich V. Irreversible electroporation therapy in the management of locally advanced pancreatic adenocarcinoma. *J Am Coll Surg*. 2012;215:361–369.
14. Scheffer HJ, Nielsen K, de Jong MC, et al. Irreversible electroporation for nonthermal tumor ablation in the clinical setting: a systematic review of safety and efficacy. *J Vasc Interv Radiol*. 2014;25:997–1011.
15. Al-Sakere B, Andre F, Bernat C, et al. Tumor ablation with irreversible electroporation. *PLoS One*. 2007;2:e1135.
16. Yarmush ML, Golberg A, Serša G, Kotnik T, Miklavčič D. Electroporation-based technologies for medicine: principles, applications, and challenges. *Annu Rev Biomed Eng*. 2014;16:295–320.
17. Jiang CL, Davalos RV, Bischof JC. A review of basic to clinical studies of irreversible electroporation therapy. *IEEE Trans Biomed Eng*. 2015;62:4–20.
18. Ellis TL, Garcia PA, Rossmeisl JH Jr, Henao-Guerrero N, Robertson J, Davalos RV. Nonthermal irreversible electroporation for intracranial surgical applications. Laboratory investigation. *J Neurosurg*. 2011;114:681–688.
19. Kotnik T, Kramar P, Pucihar G, Miklavcic D, Tarek M. Cell membrane electroporation-part 1: the phenomenon. *IEEE Electr Insul Mag*. 2012;28:14–23.
20. Haberl S, Miklavcic D, Sersa G, Frey W, Rubinsky B. Cell membrane electroporation-part 2: the applications. *IEEE Electr Insul Mag*. 2013;29:29–37.
21. Zupanic A, Kos B, Miklavcic D. Treatment planning of electroporation-based medical interventions: electrochemotherapy, gene electrotransfer and irreversible electroporation. *Phys Med Biol*. 2012;57:5425.
22. Groselj A, Kos B, Cemazar M, et al. Coupling treatment planning with navigation system: a new technological approach in treatment of head and neck tumors by electrochemotherapy. *BioMed Eng Online*. 2015;14:S2–S2.
23. Kos B, Voigt P, Miklavcic D, Moche M. Careful treatment planning enables safe ablation of liver tumors adjacent to major blood vessels by percutaneous irreversible electroporation (IRE). *Radiol Oncol*. 2015;49:234–241.
24. Edhemovic I, Gadzijev EM, Brecelj E, et al. Electrochemotherapy: a new technological approach in treatment of metastases in the liver. *Technol Cancer Res Treat*. 2011;10:475–485.
25. Sel D, Lebar AM, Miklavcic D. Feasibility of employing model-based optimization of pulse amplitude and electrode distance for effective tumor electropermeabilization. *IEEE Trans Biomed Eng*. 2007;54:773–781.
26. Miklavcic D, Semrov D, Mekid H, Mir LM. A validated model of *in vivo* electric field distribution in tissues for electrochemotherapy and for DNA electrotransfer for gene therapy. *Biochim Biophys Acta*. 2000;1523:73–83.
27. Edd JF, Davalos RV. Mathematical modeling of irreversible electroporation for treatment planning. *Technol Cancer Res Treat*. 2007;6:275–286.
28. Garcia PA, Rossmeisl JH, Neal RE II, et al. Intracranial nonthermal irreversible electroporation: in vivo analysis. *J Membr Biol*. 2010;236:127–136.
29. Miklavcic D, Snoj M, Zupanic A, et al. Towards treatment planning and treatment of deep-seated solid tumors by electrochemotherapy. *BioMed Eng Online*. 2010;9:10.
30. Garcia PA, Rossmeisl JH Jr, Neal RE 2nd, Ellis TL, Davalos RV. A parametric study delineating irreversible electroporation from thermal damage based on a minimally invasive intracranial procedure. *Biomed Eng Online*. 2011;10:34.
31. Golberg A, Rubinsky B. A statistical model for multidimensional irreversible electroporation cell death in tissue. *Biomed Eng Online*. 2010;9:13.
32. Garcia PA, Davalos RV, Miklavcic D. A numerical investigation of the electric and thermal cell kill distributions in electroporation-based therapies in tissue. *PLoS One*. 2014;9:e103083.
33. Dermol J, Miklavčič D. Mathematical models describing chinese hamster ovary cell death due to electroporation in vitro. *J Membr Biol*. 2015;248:865–881.
34. Young BD, Levine JM, Porter BF, et al. Magnetic resonance imaging features of intracranial astrocytomas and oligodendrogliomas in dogs. *Vet Radiol Ultrasound*. 2011;52:132–141.
35. Rossmeisl JH Jr, Garcia PA, Daniel GB, et al. Invited review–neuroimaging response assessment criteria for brain tumors in veterinary patients. *Vet Radiol Ultrasound*. 2014;55:115–132.
36. Åström M, Zrinzo LU, Tisch S, Tripoliti E, Hariz MI, Wårdell K. Method for patient-specific finite element modeling and simulation of deep brain stimulation. *Med Biol Eng Comput*. 2009;47:21–28.
37. Cukjati D, Batiuskaite D, Andre F, Miklavcic D, Mir LM. Real time electroporation control for accurate and safe in vivo non-viral gene therapy. *Bioelectrochemistry*. 2007;70:501–507.

38. Corovic S, Lackovic I, Sustaric P, Sustar T, Rodic T, Miklavcic D. Modeling of electric field distribution in tissues during electroporation. *BioMed Eng Online*. 2013;12:1–27.
39. Latikka J, Kuurne T, Eskola H. Conductivity of living intracranial tissues. *Phys Med Biol*. 2001;461611–1616.
40. Gabriel S, Lau RW, Gabriel C. The dielectric properties of biological tissues: III. Parametric models for the dielectric spectrum of tissues. *Phys Med Biol*. 1996;41:2271–2293.
41. Sel D, Cukjati D, Batiuskaite D, Slivnik T, Mir LM, Miklavcic D. Sequential finite element model of tissue electropermeabilization. *IEEE Trans Biomed Eng*. 2005;52:816–827.
42. Neal RE II, Garcia PA, Robertson JL, Davalos RV. Experimental characterization and numerical modeling of tissue electrical conductivity during pulsed electric fields for irreversible electroporation treatment planning. *IEEE Trans Biomed Eng*. 2012;59:1076–1085.
43. Kos B, Zupanic A, Kotnik T, Snoj M, Sersa G, Miklavcic D. Robustness of treatment planning for electrochemotherapy of deep-seated tumors. *J Membr Biol*. 2010;236:147–153.
44. Peleg M. A model of microbial survival after exposure to pulsed electric fields. *J Sci Food Agric*. 1995;67:93–99.
45. Sharabi S, Kos B, Last D, et al. A statistical model describing combined irreversible electroporation and electroporation-induced blood-brain barrier disruption. *Radiol Oncol*. 2016;50:28–38.
46. Marčan M, Pavliha D, Kos B, Forjanič T, Miklavčič D. Web-based tool for visualization of electric field distribution in deep-seated body structures and planning of electroporation-based treatments. *BioMed Eng Online*. 2015;14:S4.
47. Pucihar G, Krmelj J, Rebers M, et al. Equivalent pulse parameters for electroporation. *IEEE Trans Biomed Eng*. 2011;58:3279–3288.
48. Garcia PA, Rossmeisl JH Jr, Robertson JL, et al. 7.0-T magnetic resonance imaging characterization of acute blood-brain-barrier disruption achieved with intracranial irreversible electroporation. *PLoS One*. 2012;7:e50482.
49. Salford LG, Persson BR, Brun A, Ceberg CP, Kongstad PC, Mir LM. A new brain tumour therapy combining bleomycin with in vivo electropermeabilization. *Biochem Biophys Res Commun*. 1993;194:938–943.
50. Hjouj M, Last D, Guez D, et al. MRI study on reversible and irreversible electroporation induced blood brain barrier disruption. *PLoS One*. 2012;7:e42817.
51. Arena CB, Garcia PA, Sano MB, et al. Focal blood-brain-barrier disruption with high-frequency pulsed electric fields. *Technology*. 2014;02:206–213.
52. Bonakdar M, Wasson EM, Lee YW, Davalos RV. Electroporation of brain endothelial cells on chip toward permeabilizing the blood-brain barrier. *Biophys J* . 2016;110:503–513.
53. Arena CB, Sano MB, Rossmeisl JH, et al. High-frequency irreversible electroporation (H-FIRE) for non-thermal ablation without muscle contraction. *BioMedical Eng Online*. 2011;10:102.
54. Stupp R, Taillibert S, Kanner AA, et al. Maintenance therapy with tumor-treating fields plus temozolomide vs temozolomide alone for glioblastoma: a randomized clinical trial. *JAMA*. 2015;314:2535–2543.
55. Li X, Xu K, Li W, et al. Immunologic response to tumor ablation with irreversible electroporation. *PLoS One*. 2012;7:e48749.
56. Neal RE II, Rossmeisl JH Jr, Robertson JL, et al. Improved local and systemic anti-tumor efficacy for irreversible electroporation in immunocompetent versus immunodeficient mice. *PLoS One*. 2013;8:e64559.
57. Bastianpillai C, Petrides N, Shah T, Guillaumier S, Ahmed HU, Arya M. Harnessing the immunomodulatory effect of thermal and non-thermal ablative therapies for cancer treatment. *Tumor Biol*. 2015;36:9137–9146.
58. Zupanic A, Corovic S, Miklavcic D. Optimization of electrode position and electric pulse amplitude in electrochemotherapy. *Radiol Oncol*. 2008;42:93–101.
59. Beyer LP, Pregler B, Nießen C, et al. Stereotactically-navigated percutaneous Irreversible Electroporation (IRE) compared to conventional IRE: a prospective trial. *PeerJ*. 2016;4:e2277.
60. Kranjc M, Markelc B, Bajd F, et al. In situ monitoring of electric field distribution in mouse tumor during electroporation. *Radiology*. 2015;274:115–123.
61. Serša I, Kranjc M, Miklavčič D. Current density imaging sequence for monitoring current distribution during delivery of electric pulses in irreversible electroporation. *BioMed Eng Online*. 2015;14:S6–S6.